



Original Article

Linear and Nonlinear Magneto-optical Absorption Coefficients and Refractive Index Changes in WSe₂ Monolayer

Luong Van Tung¹, Nguyen Quang Bau², Tran Ngoc Bich^{3,4},
Pham Tuan Vinh⁵, Huynh Vinh Phuc^{5,*}

¹Sai Gon University, 273 An Duong Vuong, Ho Chi Minh City, Vietnam

²VNU University of Science, 334 Thanh Xuan, Nguyen Trai, Hanoi, Vietnam

³University of Education, Hue University, 32 Le Loi, Hue City, Vietnam

⁴Quang Binh University, 312 Ly Thuong Kiet, Dong Hoi, Quang Binh, Vietnam

⁵Dong Thap University, 783 Pham Huu Lau, Dong Thap, Vietnam

Received 02 February 2021

Revised 21 April 2021; Accepted 21 April 2021

Abstract: This work studies the linear, the third-order nonlinear, and the total optical absorption coefficients (OACs) and the refractive index changes (RICs) caused by both intra- and inter-band transitions in the WSe₂ monolayer. The expression for the OACs and RICs in the presence of a magnetic field as well as the Zeeman and electric fields are found by using the compact density matrix approach. The results show that the spin states strongly affect the OACs and RICs, which display the violet-shift behavior with the increase of the magnetic field. The Zeeman fields do not affect the peak positions but slightly reduce peak intensities. The OACs and RICs due to intra-band transition display only one peak in the THz range, while the inter-band spectra show a series of peaks in the near-infrared optical range, making monolayer WSe₂ be a promising candidate for novel optoelectronic applications.

Keywords: WSe₂ monolayer, optical absorption coefficients, refractive index changes, magnetic field.

1. Introduction

In recent years, studies on the transition metal dichalcogenides (TMDCs) have been developed rapidly due to their fascinating electronic and optical properties including the large natural band gap and

* Corresponding author.

E-mail address: hvphuc@dthu.edu.vn

<https://doi.org/10.25073/2588-1124/vnumap.4629>

the strong spin-orbit coupling (SOC) [1]. Using the equation of motion, Have et al. [2] studied the excitonic properties of TMDCs monolayer in the presence of the magnetic field where the electron-electron interaction has been taken into account. Using a Dirac-type Hamiltonian for electrons around the K and K' points, the authors have introduced the full picture for the band structure of TMDCs monolayer including the effects of the spin-orbit splitting of the bands. After that, this result has been used to study the longitudinal and the transverse susceptibilities [3].

As a member of the TMDC family, the Tungsten diselenide (WSe_2) has all its extraordinary electronic properties, such as strong SOC (its values are $\lambda_v = 0.466$ eV and $\lambda_c = 0.036$ eV in the valence and conduction bands [4]) and large nature band gap ($\Delta = 0.80$ eV [5]). That is the reason why WSe_2 has attracted research in many fields [6-8]. By executing the polarization-resolved magnetophotoluminescence, Srivastava et al. have reported observation of the valley Zeeman splitting and magnetic tuning of polarization of the excitonic valley pseudospin in monolayer WSe_2 [6]. Using an external magnetic field, the experiments that demonstrate the valley Zeeman effect-strongly anisotropic lifting of the degeneracy of the valley pseudospin degree of freedom in WSe_2 , have also been reported in detail [7]. Recently, the influence of the very strong spin-orbit coupling and the anisotropic lifting of the valley pseudospin degeneracy on the magnetotransport properties of the WSe_2 monolayer has also been studied [8]. Their results show that intraband and interband optical transitions in WSe_2 are located in two different regimes: the microwave-to-THz range for the intraband optical transitions and the visible frequency range for the interband transitions. The optical absorption coefficients (OACs) and the refractive index changes (RICs) in the layered materials have been studied widely [9-11]. When studying the optical properties of monolayer phosphorene, Nguyen et al. found that the OACs and RICs in phosphorene were strongly affected by the magnetic field. Besides, their peaks appear in two different regimes: the microwave to THz and the visible frequency. The amplitude of intra-band transition peaks is found to be larger than that of the inter-band transitions. The resonant peaks are violet-shifted with the increase of the magnetic field [9]. Similar results have also been obtained in the MoS_2 [10] and WS_2 [11] monolayers. These works show that the OACs and RICs can be used as a useful tool to study the optical properties of the WSe_2 monolayer.

In this work, we investigate the linear, third-order nonlinear, and total OACs and RICs in monolayer WSe_2 in the presence of the magnetic field. Using the expression in terms of single-particle eigenfunctions and eigenvalues of this material in the presence of the magnetic field, we calculate the OACs and RICs for both intra and inter-band transitions between the two bands. We also study the effect of the spin states as well as the magnetic, electric, and Zeeman fields on the OACs and RICs spectrum of WSe_2 monolayer.

2. Theoretical Framework

2.1. The Single-particle Electronic Model for WSe_2 Monolayer

To calculate the OACs and the RICs, we need the explicit expressions for the eigenfunctions as well as for the eigenvalues of electrons in the WSe_2 monolayer. To do this, we consider a two-dimensional WSe_2 system where carriers move freely in the (xy) plane, a uniform static magnetic field B , and an electric field E_z are applied to the z -direction. The low-energy Hamiltonian including the spin and valley Zeeman fields is given as follows [12]:

$$H_0 = v_F (\tau \sigma_x \pi_x + \sigma_y \pi_y) + (\Delta_{\tau,s} + d\Delta_z) \sigma_z + O_{\tau,s} + sM_s - \tau M_v, \quad (1)$$

where $\hbar v_F = 3.94$ (eVÅ⁰) is the Fermi energy [5], $\sigma_i (i = x, y, z)$ are the Pauli matrices, the valley index $\tau = \pm 1$ is for K and K' one, $s = \pm 1$ is for the spin up and spin down, $2d$ is the distance between the W and Se sublattices, the electric field term is $\Delta_z = eE_z$, the quantity $\vec{\pi} = \vec{p} + e\vec{A}$ is the canonical momentum with \vec{p} being the normal momentum and $\vec{A} = (0, Bx, 0)$ being the vector potential in the Landau gauge. The Dirac mass and the offset energy expressions are [3]

$$\Delta_{\tau,s} = \Delta - s\tau(\lambda_v - \lambda_c)/4, \quad (2)$$

$$O_{\tau,s} = s\tau(\lambda_c + \lambda_v)/4. \quad (3)$$

Here, $\Delta = 0.80$ eV is the intrinsic band-gap [5], the Zeeman fields are $M_j = g_j \mu_B B / 2$, with $j = s, v$ corresponding to the spin and valley ones, $\mu_B = e\hbar / 2m_e$ is the Bohr magneton with $m_e = 0.40m_0$ being the electron effective mass in WSe₂ [13], and $g_j = 2 + g'_j$ with $g'_s = 0.98$ and $g'_v = 4.34$ are the Landé factors [13]. The corresponding eigenvalues of Eq. (1) are

$$E_\lambda = E_{n,s}^{\tau,p} = pE_{n,s}^\tau + O_{\tau,s} + sM_s - \tau M_v. \quad (4)$$

In Eq. (4), the index $p = \pm 1$ refers to the conduction and valence bands, and

$$E_{n,s}^\tau = \sqrt{n(\hbar\omega_c)^2 + (\Delta_{\tau,s}^z)^2}, \quad n = 0, 1, 2, \dots, \quad (5)$$

where we have denoted $\Delta_{\tau,s}^z = \Delta_{\tau,s} + d\Delta_z$ referring to the effective Dirac mass term and $\omega_c = v_F \sqrt{2eB/\hbar}$ is the cyclotron frequency. The eigenfunctions corresponding to the Hamiltonian given in Eq. (1) are $|\lambda\rangle = e^{ik_y y} \psi_{n,s}^{\tau,p}(x) / \sqrt{L_y}$, where

$$\psi_{n,s}^{\tau,p}(x) = \begin{pmatrix} \tau A_{n,s}^{\tau,p} \phi_{n-1}(x-x_0) \\ B_{n,s}^{\tau,p} \phi_n(x-x_0) \end{pmatrix}, \quad (6)$$

with $\phi_n(x-x_0)$ are the normalization oscillator functions centered at $x_0 = \alpha_c^2 k_y$, and the normalization constants are

$$A_{n,s}^{\tau,p} = \sqrt{\frac{pE_{n,s}^\tau + \Delta_{\tau,s}^z}{2pE_{n,s}^\tau}}, \quad \text{and} \quad B_{n,s}^{\tau,p} = \sqrt{\frac{pE_{n,s}^\tau - \Delta_{\tau,s}^z}{2pE_{n,s}^\tau}}. \quad (7)$$

In the next subsection, we will use the above equations to evaluate the OACs and RICs in WSe₂ monolayer.

2.2. The Optical Absorption Coefficients and Refractive Index Changes

Using the compact density matrix approach, the linear and nonlinear optical susceptibilities for transitions between the two bands $|\lambda\rangle$ and $|\lambda'\rangle$ can be calculated as follows [11]:

$$\varepsilon_0 \chi_{xx}^{(1)}(\Omega) = \frac{1}{2\pi\hbar\alpha_c^2} \sum_{\lambda,\lambda'} \frac{(f_\lambda - f_{\lambda'}) (d_{\lambda'\lambda}^x)^* d_{\lambda\lambda'}^x}{E_{\lambda'\lambda} - \hbar\Omega - i\hbar\gamma_0}, \quad (8)$$

$$\varepsilon_0 \chi_{xx}^{(3)}(\Omega) = -\frac{1}{2\pi h \alpha_c^2} \sum_{\lambda, \lambda'} \frac{(f_\lambda - f_{\lambda'}) (d_{\lambda'\lambda}^x)^* d_{\lambda\lambda'}^x}{E_{\lambda'\lambda} - \hbar\Omega - i\hbar\gamma_0} \times \left[\frac{4(d_{\lambda'\lambda}^x)^* d_{\lambda\lambda'}^x}{(E_{\lambda'\lambda} - \hbar\Omega)^2 + (\hbar\gamma_0)^2} - \frac{(d_{\lambda'\lambda}^x - d_{\lambda\lambda'}^x)^2}{(E_{\lambda'\lambda} - i\hbar\gamma)(E_{\lambda'\lambda} - \hbar\Omega - i\hbar\gamma_0)} \right], \quad (9)$$

where $h = 3.36 \text{ \AA}$ is the thickness of the monolayer WSe₂ [14], α_c is the magnetic length, f_λ is the distribution function for an electron at the $|\lambda\rangle$ state, $E_{\lambda'\lambda} = E_{\lambda'} - E_\lambda$ with E_λ is given in Eq. (4), $\hbar\gamma_0 = 0.2\sqrt{B}$ (meV) [11], $\hbar\Omega$ is the photon energy, and $d_{\lambda\lambda'}^x$ is the dipole matrix element in the x -direction, which is given as follows:

$$d_{\lambda\lambda'}^x = -e\delta_{k_y, k_y'} \langle \psi_{n',s'}^{\tau',p'} | x | \psi_{n,s}^{\tau,p} \rangle = \frac{i\hbar v_F \tau}{E_{\lambda'\lambda}} \left[\tau' (A_{n',s'}^{\tau',p'})^* B_{n,s}^{\tau,p} \delta_{n',n+1} + \tau (B_{n',s'}^{\tau',p'})^* A_{n,s}^{\tau,p} \delta_{n',n-1} \right] \delta_{k_y, k_y'}. \quad (10)$$

From the expressions for the optical susceptibilities shown in Eqs. (8) and (9), we can find the OACs and RICs as follows [15]:

$$\alpha(\Omega, I) = \alpha^{(1)}(\Omega) + \alpha^{(3)}(\Omega, I), \quad (11)$$

$$\alpha^{(k)}(\Omega, I) = \Omega \sqrt{\frac{\mu}{\varepsilon_R}} \text{Im} \left[\varepsilon_0 \chi_{xx}^{(k)}(\Omega) \right], \quad (12)$$

$$\frac{\Delta n(\Omega, I)}{n_r} = \frac{\Delta n^{(1)}(\Omega)}{n_r} + \frac{\Delta n^{(3)}(\Omega, I)}{n_r}, \quad (13)$$

$$\frac{\Delta n^{(k)}(\Omega, I)}{n_r} = \text{Re} \left[\frac{\chi_{xx}^{(k)}(\Omega) \tilde{E}^{(k-1)}}{2n_r^2} \right], \quad (14)$$

Here, $k = 1, 3$ for the linear and nonlinear terms, μ is the permeability of the material, $\varepsilon_R = n_r^2 \varepsilon_0$ with ε_0 being the permittivity of the vacuum and $n_r = 5.68$ being the refractive index of the WSe₂ material [16], and $I = 3 \times 10^6 \text{ W/m}^2$ is the light intensity.

3. Results and Discussion

In this section, we provide detailed numerical evaluation of the linear, the nonlinear, and the total OACs and RICs in WSe₂ monolayer. The parameters are shown as they appear. Since the K and K' valleys are similar, in this section, we will only focus on the K valley and put $\tau = \tau' = 1$ in all calculations. It is noted that although we would only evaluate for the K valley, the result could also be validated for the K' one. The following results will evaluate both intra- and interband transitions.

3.1. The Intraband Transitions

In this subsection, we present the results for the OACs and RICs due to intraband transition ($p = p' = 1$). Due to the Delta Kronecker contained in the dipole matrix element shown in Eq. (10),

only the transitions, which satisfy the condition $\Delta n = n' - n = \pm 1$, are allowed. Therefore, the absorbed photon energy caused by the intraband transition is given as

$$\hbar\Omega_{\text{intra}} = E_{\lambda'\lambda} = \frac{(\hbar\omega_c)^2}{2[\Delta_{\tau,s} + d\Delta_z]} = \frac{(\hbar\omega_c)^2}{2[\Delta - s(\lambda_v - \lambda_c)/4 + d\Delta_z]}. \quad (15)$$

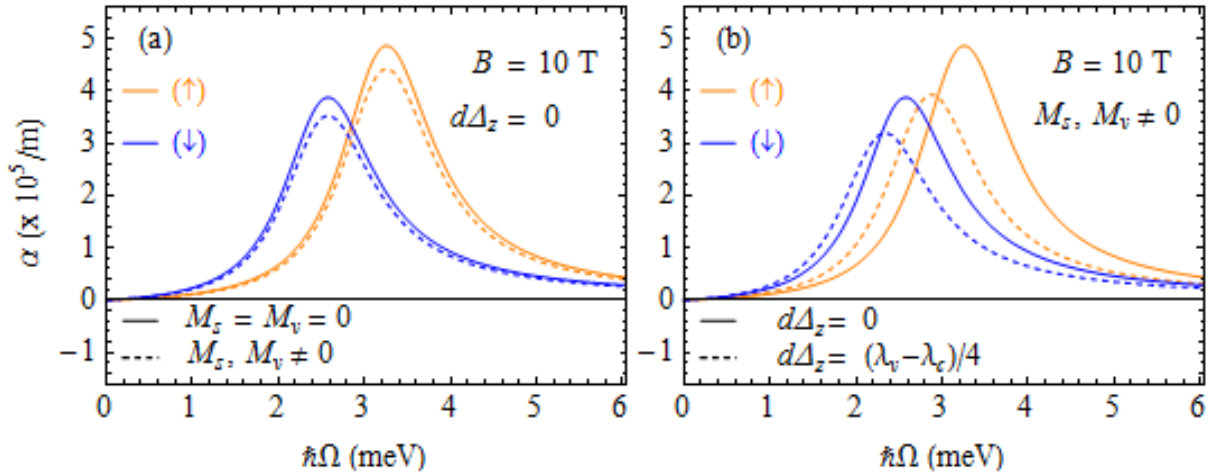


Figure 1. The dependence on the photon energy of the linear OACs due to intraband transitions for two different states of spin at $B = 10$ T, for different effects: (a) the Zeeman fields; (b) the electric field.

In Figure 1, we show the linear OACs due to intraband transitions versus photon energy at a certain value of the magnetic field including the effects of the Zeeman and electric fields. It is clear from Eq. (15) that the $\hbar\Omega_{\text{intra}}$ is independent of the Landau levels index, i.e., all the intraband transition peaks located at the same position in the THz range of the electromagnetic spectrum. As a result, in the case of intraband transitions, there is only one resonant peak observed for each state of spin. Due to strong SOC in WSe₂ monolayer, the spin state significantly affects OACs not only in their intensities but also in their positions: the OAC peaks due to the spin-up state are higher and locate on the right-hand side in comparison to those due to the spin-down state. For the WSe₂ monolayer, we have $\lambda_v - \lambda_c = 430$ meV, leading to $\Delta_{1,\uparrow} < \Delta_{1,\downarrow}$. Using this relation into Eq. (15), we have $\hbar\Omega_{\text{intra}}(\uparrow) > \hbar\Omega_{\text{intra}}(\downarrow)$. That is the reason why the peaks due to the spin-up state are located on the right-hand side of those caused by the spin-down state as observed in Figure 1.

The effect of the Zeeman fields and electric field on the linear OACs is depicted in Figure 1a and Figure 1(b), respectively. The value of the electric field of $d\Delta_z = (\lambda_v - \lambda_c)/4 = 107.5$ meV is chosen to cancel the SOC term in the $K \uparrow$ and $K \downarrow$ states. We can see from Eq. (15) that the $\hbar\Omega_{\text{intra}}$ does not depend on the Zeeman fields but is proportional to $(d\Delta_z)^{-1}$. Therefore, the Zeeman fields do not affect the peak positions, but slightly reduce their intensities as shown clearly in Figure 1(a). Meanwhile, when the electric field is taken into account ($d\Delta_z \neq 0$), the denominator in Eq. (15) increases, leading to the decrease of the $\hbar\Omega_{\text{intra}}$. As a result, the peak positions shift to the lower energy region (red-shift)

as shown in Figure 1b. These results are the same as those in MoS₂ [9] and WS₂ [11] monolayers as they are all members of the TMDC family. Besides, with much stronger SOC in the WSe₂ monolayer, the absorbed photon energy in this material is slightly bigger than that in the MoS₂ monolayer [9].

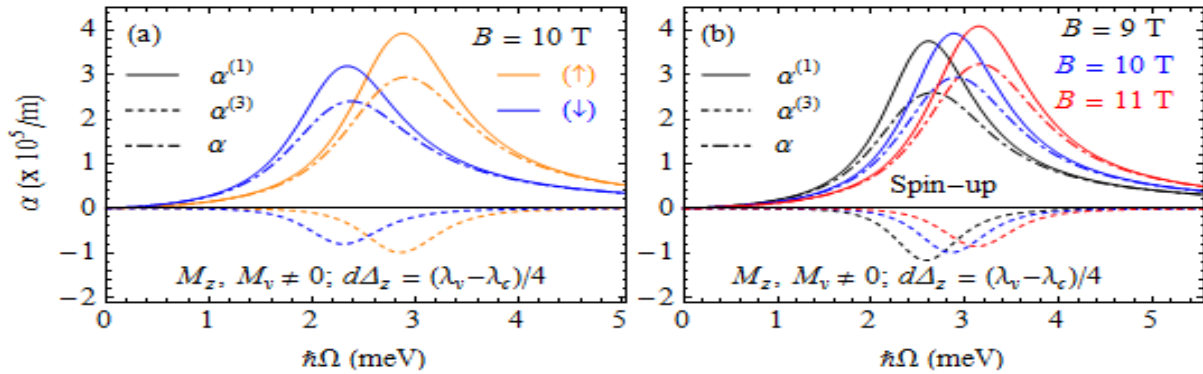


Figure 2. The dependence on the photon energy of the linear, the third-order nonlinear, and the total OACs due to intraband transitions including the Zeeman and electric fields: (a) at $B = 10$ T; (b) different values of B .

In Figure 2a, the linear, the third-order nonlinear, and the total OACs due to intraband transitions are shown as a function of photon energy at $B = 10$ T for two states of spin. The results include the effects of the Zeeman and electric fields. It is seen that, both $\alpha^{(1)}$ and $\alpha^{(3)}$ are located at the same position, with the peak positions are given in Eq. (15), leading to the fact that the peak of the total OAC also has the same position as those of $\alpha^{(1)}$ and $\alpha^{(3)}$. Because of its negative value, when the nonlinear term is taken into account, it reduces the total one in comparison to the linear OAC. Because the results for the OACs caused by spin-up and spin-down states are similar, in the following, we only analyze for the spin-up state but the results for spin-down one are also validated. The effect of the magnetic field on the OACs is presented in Figure 2b. We can see that when the magnetic field increases the intensities of the resonant peaks are enhanced and their peak positions are shifted to the higher energy region (the violet-shift). The violet-shifted behavior of the resonant peaks can be understood from the increase of the cyclotron energy when the magnetic field increases. Indeed, we can see from Eq. (15) that with the increase of the magnetic field, the $\hbar\omega_c$ will increase, leading to the enhancement of the $\hbar\Omega_{\text{intra}}$.

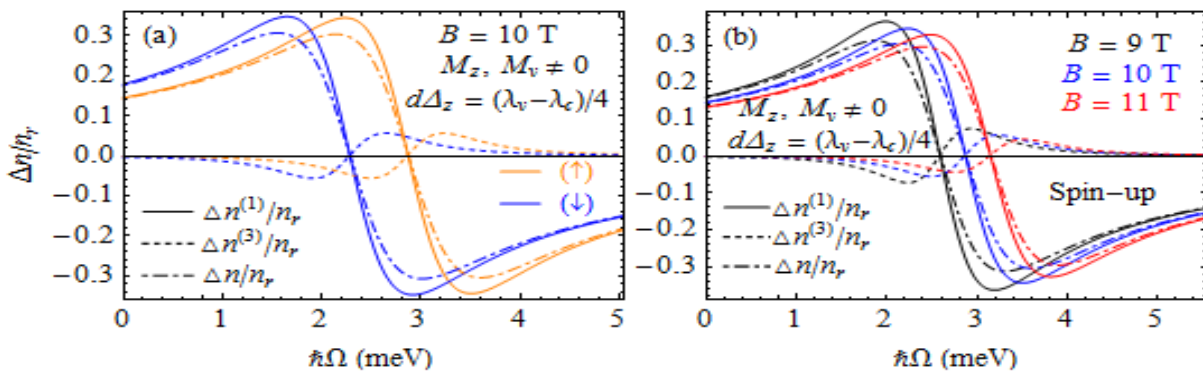


Figure 3. The dependence on the photon energy of the linear, the third-order nonlinear, and the total RICs due to intraband transitions including the Zeeman and electric fields: (a) at $B = 10$ T; (b) different values of B .

The dependence of the linear, the third-order nonlinear, and the total RICs on the photon energy is shown in Figure 3. We see that the behaviors of the RICs in Figure 3a and Figure 3b are similar to that of the OACs shown in Figure 2. This means that there is only one peak located in the THz range for each state of the spin. Besides, the contribution of the nonlinear term reduces the intensity of the total term. This is because of the opposite sign between the linear and the nonlinear terms. The effect of the magnetic field on the RICs is illustrated in Figure 3b. We can see that when the magnetic field increases, the RICs spectrum reduces and shifts to the higher energy region (violet-shift) due to the increase of the cyclotron energy. These results are in agreement with the results for the conductivity in graphene [17] and silicene [18] as well as the results for the OACs and RICs in MoS₂ [10] and WS₂ [11] monolayers.

3.2. The Interband Transitions

For the interband transitions, the absorbed photon energies are given as follows:

$$\hbar\Omega_{inter} = \frac{(2n+1)(\hbar\omega_c)^2}{2[\Delta - s(\lambda_v - \lambda_c)/4 + d\Delta_z]} + 2[\Delta - s(\lambda_v - \lambda_c)/4 + d\Delta_z]. \quad (16)$$

In contrast to the intraband transition case shown in Eq. (15), the $\hbar\Omega_{inter}$ is proportional to the Landau level index. Therefore, the peak positions generated by different LLs do not coincide but shift gradually to the right-hand side with the increase of the LLs indices. Besides, the $\hbar\Omega_{inter}$ is also found to be proportional to $2\Delta = 1.6$ eV, leading to the fact that the absorption spectra due to the interband transition are in the near-infrared region. All these interesting results will be presented in the following.

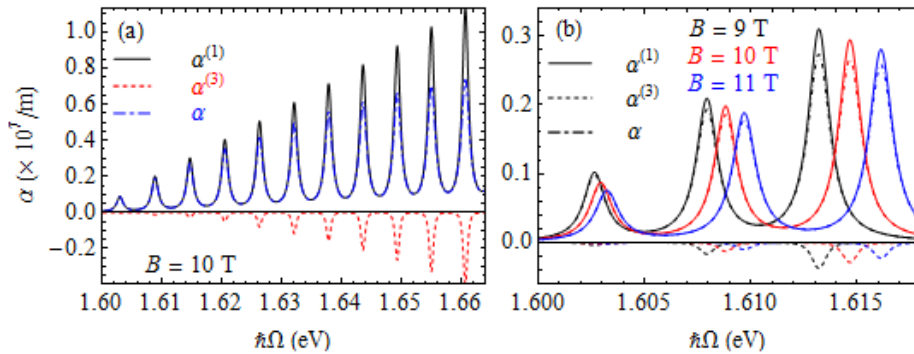


Figure 4. The dependence on the photon energy of the linear, the third-order nonlinear, and the total OACs due to interband transitions at $M_z, M_v \neq 0, d\Delta_z = (\lambda_v - \lambda_c)/4$: (a) at $B = 10$ T; (b) different values of B .

Figure 4 shows the OACs due to interband transitions as a function of photon energy at $B = 10$ T (Figure 4a) and at different values of the magnetic fields (Figure 4b). The results are evaluated in the presence of the electric and Zeeman fields. As analyzed above, the interband spectra appear in a series of peaks due to the dependence of the $\hbar\Omega_{inter}$ on the LLs index. When the magnetic field increases, the peak positions shift to the higher energy region caused by the increase of the cyclotron energy. Besides, the peak intensities in the case of the interband transitions are much higher than those in the case of the intraband transitions, being in good agreement with the results reported in the MoS₂ [10] and WS₂ [11] monolayers.

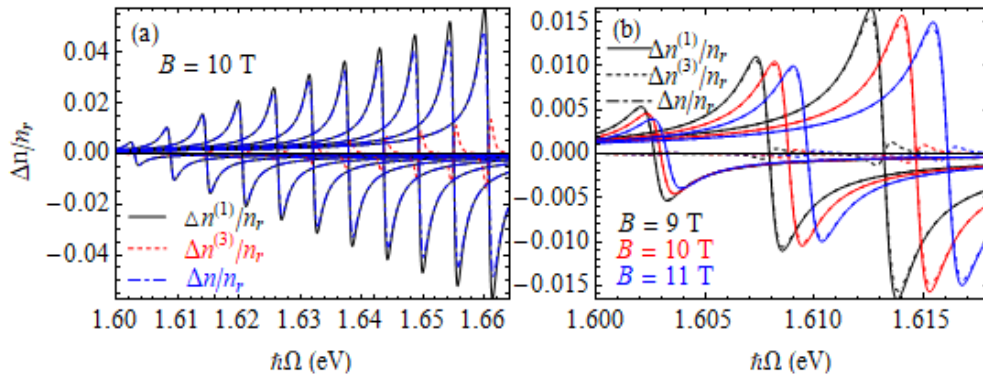


Figure 5. The dependence on the photon energy of the linear, the third-order nonlinear, and the total RICs due to interband transitions at $M_z, M_v \neq 0, d\Delta_z = (\lambda_v - \lambda_c)/4$: (a) at $B = 10$ T, (b) different values of B .

Figure 5 shows the RICs for the interband transitions including the effects of the Zeeman and electric fields. Similar to the case of the interband transition OACs, the RICs for the interband transitions also display a series of peaks but with smaller intensities in comparison to the intraband transition ones. The violet-shift behavior with the increase of the magnetic field is also observed in Figure 5b, which is the result of the enhancement of the cyclotron energy, similar to the case of the OACs shown in Figure 4b. Finally, the intensities of the RICs obtained here are in the same order as those obtained in MoS₂ [10] and WS₂ [11] monolayers but are bigger than those obtained in phosphorene [9]. A similar feature between the MoS₂, WS₂, and the WSe₂ comes from the fact that all of them are members of the TMDC family, which have a wide nature bandgap and strong SOC in comparison to those of the graphene and phosphorene. This reveals that the TMDC materials, including WSe₂, would be potential candidates for applications in the manufacture of optoelectronic devices in the near future.

4. Conclusion

We have presented the results of the study on the linear, the third-order nonlinear, and the total OACs and RICs in the WSe₂ monolayer in the presence of the perpendicular magnetic field. The results include the effects of the Zeeman and electric fields. The results show that the spin states strongly affect the OACs and RICs spectra due to the strong SOC in WSe₂ material. When the electric field is taken into account, the absorption spectra give a red-shift and reduce their intensities. The Zeeman fields do not change the peak positions but slightly reduce the peak intensities. With the increase of the magnetic field, the absorption spectra display a violet shift. The absorption spectra display only one peak in the case of intraband transitions while they show a series of peaks in the case of the interband one. Our results provide an interesting possibility to replace graphene with WSe₂ in the manufacture of optoelectronic devices.

Acknowledgments

This research was funded by Vietnam National Foundation for Science and Technology Development (NAFOSTED) under Grant 103.01-2019.11.

References

- [1] D. Xiao, G. B. Liu, W. Feng, X. Xu, W. Yao, Coupled Spin and Valley Physics in Monolayers of MoS₂ and Other Group-VI Dichalcogenides, *Phys. Rev. Lett.*, Vol. 108, 2012, pp. 196802, <https://doi.org/10.1103/PhysRevLett.108.196802>.
- [2] J. Have, G. Catarina, T. G. Pedersen, N. Peres, Monolayer Transition Metal Dichalcogenides in Strong Magnetic Fields: Validating the Wannier Model Using a Microscopic Calculation, *Phys. Rev. B*, Vol. 99, 2019, pp. 035416, <https://doi.org/10.1103/PhysRevB.99.035416>.
- [3] G. Catarina, J. Have, J. F. Rossier, N. M. Peres, Optical Orientation with Linearly Polarized Light in Transition Metal Dichalcogenides, *Phys. Rev. B*, Vol. 99, 2019, pp. 125405, <https://doi.org/10.1103/PhysRevB.99.125405>.
- [4] G. B. Liu, W. Y. Shan, Y. Yao, W. Yao, D. Xiao, Three-band Tight-binding Model for Monolayers of Group-VIB Transition Metal Dichalcogenides, *Phys. Rev. B*, Vol. 88, 2013, pp. 085433, <https://doi.org/10.1103/PhysRevB.88.085433>.
- [5] D. Xiao, G. B. Liu, W. Feng, X. Xu, W. Yao, Coupled Spin and Valley Physics in Monolayers of MoS₂ and Other Group-VI Dichalcogenides, *Phys. Rev. Lett.*, Vol. 108, 2012, pp. 196802, <https://doi.org/10.1103/PhysRevLett.108.196802>.
- [6] G. Aivazian, Z. Gong, A. M. Jones, R. L. Chu, J. Yan, D. G. Mandrus, C. Zhang, D. Cobden, W. Yao, X. Xu, Magnetic Control of Valley Pseudospin in Monolayer WSe₂, *Nat. Phys.*, Vol. 11, 2015, pp. 148-152, <https://doi.org/10.1038/nphys3201>.
- [7] A. Srivastava, M. Sidler, A. V. Allain, D. S. Lembke, A. Kis, A. Imamoglu, Valley Zeeman Effect in Elementary Optical Excitations of Monolayer WSe₂, *Nat. Phys.* Vol. 11, 2015, pp. 141-147, <https://doi.org/10.1038/nphys3203>.
- [8] M. Tahir, P. Vasilopoulos, Magneto-optical Transport Properties of Monolayer WSe₂, *Phys. Rev. B*, Vol. 94, 2016, pp. 045415, <https://doi.org/10.1103/PhysRevB.101.045424>.
- [9] C. V. Nguyen, N. N. Hieu, C. A. Duque, D. Q. Khoa, N. V. Hieu, L. V. Tung, H. V. Phuc, Linear and Nonlinear Magneto-optical Properties of Monolayer Phosphorene, *J. Appl. Phys.*, Vol. 121, 2017, pp. 045107, <https://doi.org/10.1063/1.4974951>.
- [10] C. V. Nguyen, N. N. Hieu, D. Muoi, C. A. Duque, E. Feddi, H. V. Nguyen, L. T. Phuong, B. D. Hoi, H. V. Phuc, Linear and Nonlinear Magneto-optical Properties of Monolayer MoS₂, *J. Appl. Phys.*, Vol. 123, 2018, pp. 034301, <https://doi.org/10.1063/1.5009481>.
- [11] P. T. Huong, D. Muoi, T. N. Bich, H. V. Phuc, C. Duque, P. T. N. Nguyen, C. V. Nguyen, N. N. Hieu, L. T. Hoa, Intra-and Inter-band Magneto-optical Absorption in Monolayer WS₂, *Physica E: Low-dimensional Systems and Nanostructures*, Vol. 124, 2020, pp. 114315, <https://doi.org/10.1016/j.physe.2020.114315>.
- [12] N. D. Hien, C. V. Nguyen, N. N. Hieu, S. Kubakaddi, C. Duque, M. M. Ramos, L. Dinh, T. N. Bich, H. V. Phuc, Magneto-optical Transport Properties of Monolayer Transition Metal Dichalcogenides, *Phys. Rev. B*, Vol. 101, 2020, pp. 045424, <https://doi.org/10.1103/PhysRevB.101.045424>.
- [13] A. Kormányos, V. Zolyomi, N. D. Drummond, G. Burkard, Spin-orbit Coupling, Quantum Dots, and Qubits in Monolayer Transition Metal Dichalcogenides, *Phys. Rev. X*, Vol. 4, 2014, pp. 011034, <https://doi.org/10.1103/PhysRevX.4.011034>.
- [14] Y. Ding, Y. Wang, J. Ni, L. Shi, S. Shi, W. Tang, First Principles Study of Structural, Vibrational and Electronic Properties of Graphene-like MX₂ (M= Mo, Nb, W, Ta; X= S, Se, Te) Monolayers, *Physica B: Condensed Matter*, Vol. 406, 2011, pp. 2254-2260, <https://doi.org/10.1016/j.physb.2011.03.044>.
- [15] G. Rezaei, M. Karimi, A. Keshavarz, Excitonic Effects on the Nonlinear Intersubband Optical Properties of a Semi-parabolic One-dimensional Quantum Dot, *Physica E: Low-dimensional Systems and Nanostructures*, Vol. 43, 2010, pp. 475-481, <https://doi.org/10.1016/j.physe.2010.08.035>.
- [16] H. L. Liu, C. C. Shen, S. H. Su, C. L. Hsu, M. Y. Li, L. J. Li, Optical Properties of Monolayer Transition Metal Dichalcogenides Probed by Spectroscopic Ellipsometry, *Appl. Phys. Lett.*, Vol. 105, 2014, pp. 201905, <https://doi.org/10.1063/1.4901836>.
- [17] T. Morimoto, Y. Hatsugai, H. Aoki, Optical Hall Conductivity in Ordinary and Graphene Quantum Hall Systems, *Phys. Rev. Lett.*, Vol. 103, 2009, pp. 116803, <https://doi.org/10.1103/PhysRevLett.103.116803>.
- [18] C. J. Tabert, E. J. Nicol, Valley-spin Polarization in The Magneto-optical Response of Silicene and Other Similar 2D Crystals, *Phys. Rev. Lett.*, Vol. 110, 2013, pp. 197402, <https://doi.org/10.1103/PhysRevLett.110.197402>.